Biochemistry

pubs.acs.org/biochemistry
Article

α-Helical Structure of Antimicrobial Peptides Enhances Their Activity through Molecular Surface Signatures

Michael Quagliata, Joshua Grabeck, Kathrin König, Anna Maria Papini, Paolo Rovero, Ines Neundorf, and Daniel Friedrich*

Cite This: *Biochemistry* 2025, 64, 3311−3321

ABSTRACT: The increase in antibacterial resistance is one of the greatest challenges in modern medicine, driving an urgent need to develop new drugs to combat resistant pathogens. Peptides represent a promising class of molecules that can be efficiently designed to exhibit high antimicrobial efficacy. Recently, we have highlighted how prestructuring by a triazolyl-bridge significantly enhances the activity of an antimicrobial peptide. To learn more from these findings, the aim of this study is to relate the NMR-based structure of a triazolyl-bridged peptide to its antimicrobial activity against Gram-positive and Gram-negative bacteria in comparison to its linear analogues. As we show, the triazole modification indeed induces a well-defined α-helical structure, resulting in an improved positive electrostatic surface potential on one side of the peptide and clustering of hydrophilic and hydrophobic residues on opposite surface areas of the molecule. Systematic alanine substitution further suggested that the side chains of arginine 3 and 7 and of asparagine 11 have a stronger productive impact on antimicrobial activity than those of lysine 4, 8, and 12. As shown by micelle-bound peptide structures determined by NMR, we identify arginine 3 and asparagine 11 as presumable membrane-interacting residues. Collectively, our NMR-based analysis provides evidence that an α-helical structure enhances antimicrobial activity by creating positively charged and hydrophilic, and hydrophobic areas as molecular surface signatures, potentially promoting the interaction of the peptide with the cellular target membrane.

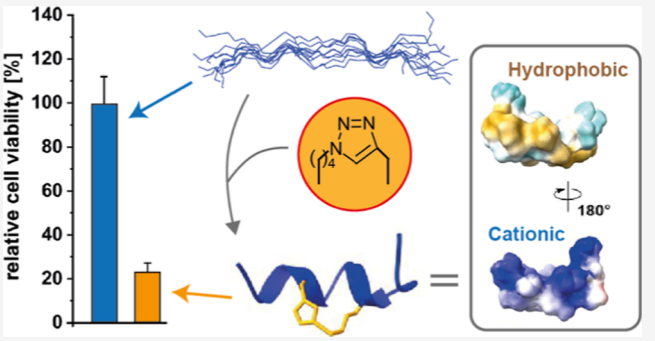

INTRODUCTION

The discovery of antibiotics revolutionized the field of medicine; however, the extensive use of these substances has led to the spread of increasingly resistant bacteria. To date, the phenomenon of antibiotic resistance is considered one of the greatest challenges in modern medicine and the development of new molecules with antibacterial activity has become a priority in biomedical research.[1−3] So-called antimicrobial peptides (AMPs) represent a promising class of such antibacterial substances as they are easy to design and can be rapidly synthesized with optimal purity and high yield.[4] In recent years, the use of peptides as therapeutics has increased, thanks to the development of solid-phase peptide synthesis (SPPS). This methodology allows one to obtain peptide sequences in large quantities and within relatively short timescales. The modular nature of these molecules facilitates modifications to tune molecular features, which is a significant advantage in the design of therapeutics.[4] However, one of the challenges of using peptides as therapeutics is their low stability in the cellular environment, where they can be easily hydrolyzed by proteases.[5] In recent years, strategies have been developed to increase proteolytic stability and thus improve pharmacokinetics, such as through the synthesis of retro-inverso (ri) peptides, the use of non-natural amino acids, or the insertion of staples.[6−9] As mentioned above, AMPs have emerged as promising molecules to tackle antibiotic resistance.[10] Many of these peptides are characterized by the high content of positively charged residues such as lysine and arginine and therefore have a net positive charge at physiological pH.[11,12] In addition, AMPs often consist of nearly 50% hydrophobic residues and thus exhibit important amphipathic properties.[13] Thanks to these characteristics, such peptides are capable of interacting with negatively charged moieties in bacterial cell surface phospholipids, thereby disrupting the integrity of the target membranes. Another class of peptides that may have properties similar to those of AMPs is cell-penetrating peptides (CPPs). CPPs are usually short peptides with the ability to cross cellular membranes and to carry attached cargoes inside cells while exhibiting minimal

Received: February 21, 2025
Revised: May 23, 2025
Accepted: June 19, 2025
Published: July 13, 2025

https://doi.org/10.1021/acs.biochem.5c00101
Biochemistry 2025, 64, 3311−3321

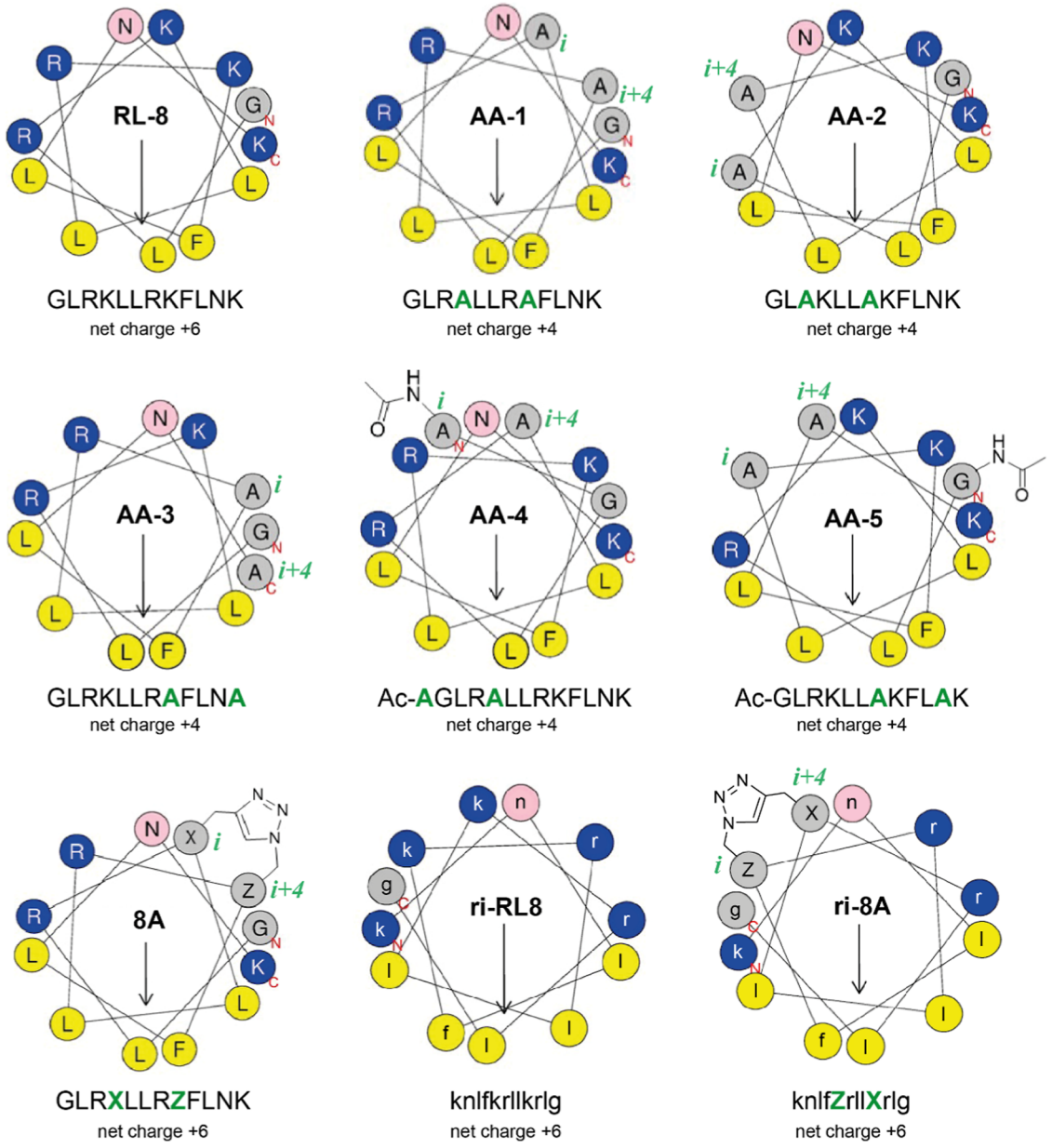

Figure 1. Helical wheel projections of designed and analyzed peptides. The N- and C-termini are indicated by red upper-case letters, and amino acids are reported using one-letter code in upper-case (in the retro-inverso peptides ri-RL8 and ri-8A in lower-case). Positively charged residues are highlighted in blue, asparagine 11 (asparagine 2 in the retro-inverso peptides) in pink, hydrophobic residues in yellow, and all other residues in gray. Acetylation and the triazolyl-bridge are depicted by their chemical structures, and L-propargylglycine and L-ε-azido-norleucine are X and Z, respectively. Modified amino acid positions are indicated by *i* and *i* + 4 (in green) to highlight the distance in the peptide sequence.

toxicity.[14,15] Like AMPs, they are often composed of basic residues and display amphipathic structures, and some of them are also able to interfere with bacterial cell membranes.[16] Recently, we have shown how we can tailor the antimicrobial activity of a CPP in a rational multistep approach of amino acid substitution.[17] Moreover, in our previous studies, we have seen that the alternation of basic and hydrophobic residues and a well-defined secondary structure allows to significantly improve amphipathic properties and thus membrane-activity in general.[18] Following this, we demonstrated that stabilization of an amphipathic α-helix by installing a side-chain-to-side-chain triazolyl-bridge (Scheme S1) in the basic and hydrophilic part of one of our hit peptides (namely, RL-8 and leading to peptide 8A) resulted in significantly higher antimicrobial activity compared to the corresponding linear peptide.[19] In fact, 8A demonstrated remarkable activity against Gram-positive and Gram-negative bacteria as well as pathogenic bacterial species. On the other side, when the triazolyl-bridge was installed in the hydrophobic part of the peptide, the antimicrobial activity was drastically reduced. Therefore, balancing out structural aspects with physicochemical properties might be strategic to developing peptides with improved antimicrobial activity. Inspired by these considerations, we were eager to evaluate the importance of chemical features for the structure and antimicrobial activity of peptide 8A. Therefore, we performed an alanine-scan at amino acid positions *i* and *i* + 4 in the basic and hydrophilic part of the linear parent peptide RL-8 (Figure 1), while maintaining its net charge, and tested all new variants for antimicrobial activity. Furthermore, we aimed to define in more detail the structure

https://doi.org/10.1021/acs.biochem.5c00101
Biochemistry 2025, 64, 3311−3321

of the triazolyl-bridged peptide 8A by NMR spectroscopy to correlate the structure with antimicrobial activity. As it is a promising candidate for further optimization toward highly potent and selective antimicrobial peptides, structural studies may help to explore potential for chemical modification and to provide the basis for establishing the mechanism of its antimicrobial function. Our results do indeed highlight how we can explain the biological activity of AMPs by careful structure−activity-relation studies.

MATERIALS AND METHODS

Peptide Synthesis. All peptides were synthesized on Rink amide resin by automated SPPS on a multiple Syro II peptide synthesizer (MultiSyntech, Witten, Germany), while the triazolyl-bridged and retro-inverso peptides were synthesized with the PurePep Chorus (Tucson, AZ, USA) following the Fmoc/*t*Bu-strategy. The following Fmoc-amino acids were used: Fmoc-Ala-OH, Fmoc-Phe-OH, Fmoc-Gly-OH, Fmoc-Lys(Boc)-OH, Fmoc-Leu-OH, Fmoc-Asn(Trt)-OH, Fmoc-Arg(Pbf)-OH, Fmoc-Nle(ε-N3)-OH, and Fmoc-Pra-OH. Fmoc deprotections were performed with a solution of 20% piperidine in DMF. Peptide assembly was performed by repeating twice the SPPS standard coupling cycle for each amino acid, using Fmoc-protected amino acids (8 equiv in DMF), OxymaPure (8 equiv in DMF), and DIC (8 equiv in DMF). N-acetylation was eventually performed using a solution of 10% Ac_2O in DMF solution for 10 min at room temperature. The triazolyl-bridge in the peptides 8A and ri-8A was installed exploiting the CuAAC click reaction as reported elsewhere.[20,21] Briefly, the resin charged with the all-protected Fmoc-peptide was treated with CuBr, 2,6-lutidine, and sodium ascorbate in DMSO:DMF (1:2) for 10 min under microwave irradiation (55 °C, 60 W). Final cleavage and side-chain deprotections were performed using a mixture of TFA/TIS/H_2O (95:2.5:2.5, v/v/v) at room temperature. After 3 h, the resin was filtered off. The peptides were precipitated with cold Et_2O and centrifuged and lyophilized. Purification of peptides was achieved by preparative reverse-phase HPLC on a C18 column and analyzed by analytical HPLC ESI-MS (LTQ XL, Thermo Scientific, Waltham, MA, USA) (Figures S1−S9).

Antimicrobial Activity Assay. In order to test the peptides for antimicrobial activity, we set up an assay analyzing the efficacy against *Bacillus spizizenii* (ATTC 6633, *B. spizizenii* subspecies *spizizenii*) and *Salmonella typhimurium* (TA100). Bacterial cultures with an optical density of more than 0.7 at 600 nm were used. In a 96-well plate, 180 μL of minimal-medium (10 mM Tris, 5 mM glucose), 10 μL of bacterial suspension, and 10 μL of peptide solution were mixed. The resulting cultures were screened at several different peptide concentrations ranging from 0.1 to 25 μM (in triplicates). To test the assay, pure H_2O and Ciprofloxacin at a concentration of 5 mg/mL were used as negative and positive controls, respectively (data not shown). All samples were then incubated at 37 °C for 4 h. Afterward, 10 μL of a 1 mg/mL solution of iodonitrotetrazolium chloride in pure DMSO was added to each well, and samples were further incubated for 15 min at 37 °C. Finally, the absorption of formazan at 560 nm in each well was measured using a Tecan infinite M200 plate reader (Tecan Group AG, Männedorf, Switzerland).

NMR Spectroscopy. NMR experiments were performed on a Bruker Avance III HDX 500 MHz NMR spectrometer equipped with a cryogenically cooled 5 mm $^1H/^{13}C/^{15}N$ TCI-probe. For each peptide sample, approximately 10 mg of peptide was dissolved in 90% H_2O/10% D_2O, and all NMR spectra were recorded at 298 K. For NMR experiments on analysis of peptide−micelle interactions, 10 mg of peptide was dissolved in 90% H_2O/10% D_2O and 10 mM *n*-dodecyl-β-D-maltopyranoside (*n*-dodecylphosphocholine, DPC, the critical micelle concentration is 1.5 mM). Resonance assignments were achieved via a set of scalar coupling-based spectra ($^1H,^1H$-TOCSY, $^1H,^{13}C$-HSQC, and $^1H,^{15}N$-HSQC), and structures were calculated based on two-dimensional $^1H,^1H$-NOESY experiments. $^1H,^1H$-TOCSY experiments using WATERGATE solvent suppression were recorded with 100 ms mixing time and 32 scans, and 204 and 128 ms were acquired in the direct and indirect dimensions, respectively (spectral widths of 10 ppm in both dimensions were used). $^1H,^{13}C$-HSQC spectra were acquired using water flip-back and WATERGATE with 128 scans for aliphatic carbons. 146 ms were recorded in the ^1H dimension at a spectral width of 14 ppm, and 17 ms at a spectral width of 60 ppm in the ^{13}C dimension. $^1H,^{15}N$-HSQC experiments using water flip-back and WATERGATE were recorded with 64 scans and 146 ms at a spectral width of 14 ppm in the ^1H dimension and 126 ms at a spectral width of 80 ppm in the ^{15}N dimension. $^1H,^1H$-NOESY spectra were acquired with water flip-back and WATERGATE, 32 scans, a mixing time of 500 ms, and 204 ms and 128 ms were acquired in the direct and indirect dimensions, respectively (spectral widths of 10 ppm in both dimensions were used). All spectra were processed using TopSpin version 3.6 and analyzed using MestreNova. Structures were calculated using Artificial Intelligence for NMR Applications (ARTINA) on the NMRtist cloud computing service, employing FLYA automated chemical shift assignment and structure calculation with CYANA.[22,23] All observed chemical shifts and their assignments were checked manually and are listed in the Supporting Information (Tables S2−S6, S9, and S10).

CD Spectroscopy. CD spectra of the peptides were recorded using quartz cells of 0.1 cm path length with a JASCO J-715 CD spectropolarimeter (JASCO, Pfungstadt, Germany) in an N_2 atmosphere at 20 °C. Each spectrum was measured in the 260−190 nm spectral range, 2 nm bandwidth, 3 accumulations, and 50 nm/min scanning speed. The peptides were dissolved in H_2O or H_2O:TFE 1:1 (v/v) at a concentration of 20 μM.

Preparation of Giant Unilamellar Vesicles and Fluorescence Microscopy. To prepare GUVs, a thin agarose film was formed on a microscope slide by melting 1% (w/v) super low-melting agarose in deionized water using a microwave. A volume of 200 μL was spread out and dried at 50 °C for 30 min on a heating plate. Subsequently, 10 μL of a lipid mixture (1,2-Dioleoyl-*sn*-glycero-3-phospho-rac-1-glycerol (DOPG) and 1,2-Dioleoyl-*sn*-glycero-3-phosphoethanolamine (DOPE) in 1:1 molar ratio) containing 0.2 mol % Atto550 was applied to the agarose layer, evenly distributed, and dried under vacuum in an exicator for 60 min to remove chloroform. A sealing ring was placed around the dried, stained lipid film, which was then hydrated with 150 μL of dextran buffer (10 mM HEPES, pH 7.4, 50 mM KCl, 50 mM NaCl, 1 mg/mL dextran) containing 3 μL of Oyster405 (Luminaris GmbH, Münster, Germany) for encapsulation of the blue dye. Slides were incubated at room temperature for 2 h. After incubation, GUVs were harvested by centrifugation at 20,000*g* for 10 min. The supernatant was discarded, and the pellet was resuspended in 300 μL of fresh dextran buffer. For

https://doi.org/10.1021/acs.biochem.5c00101
Biochemistry 2025, 64, 3311−3321

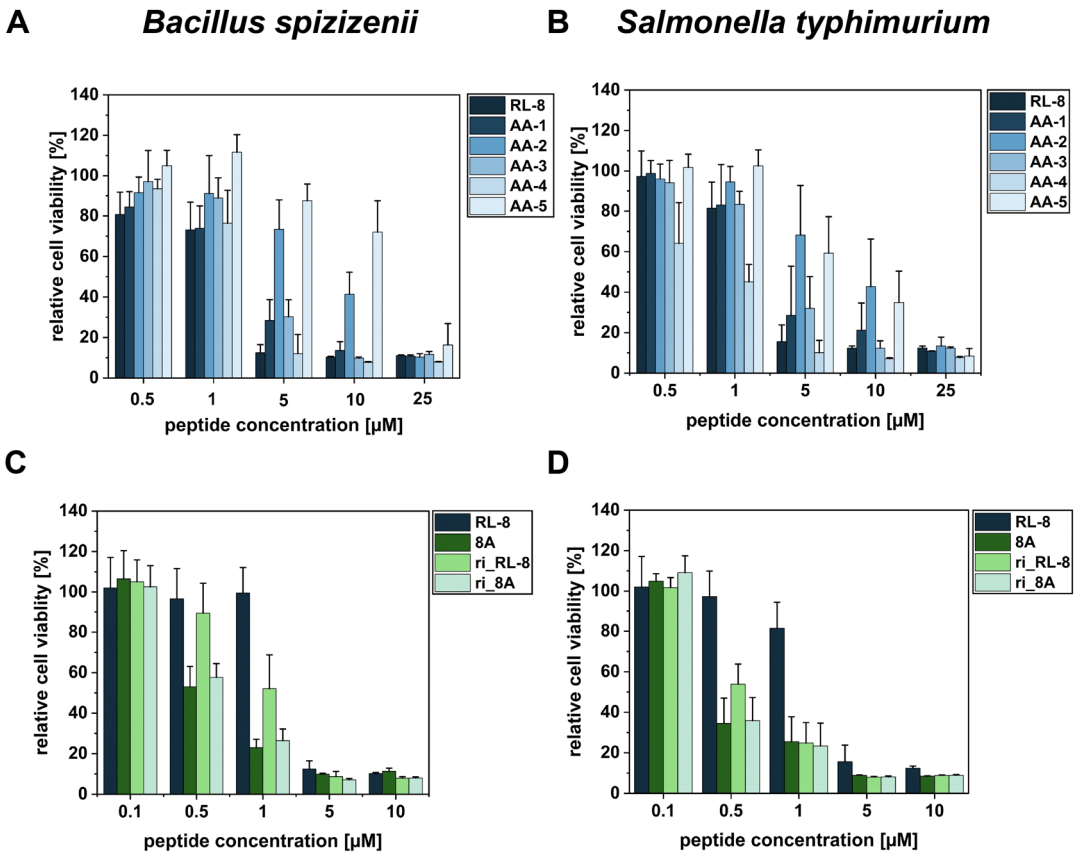

Figure 2. All peptides were tested for antimicrobial activity, as measured by the relative cell viability of *B. spizizenii* (A and C) and *S. typhimurium* (B and C). Note the different ranges of peptide concentration testing RL-8 and AA-1 through AA-5 in panels (A) and (B) and RL-8, 8A, ri-RL-8, and ri-8A in panels (C) and (D).

fluorescence microscopy, 40 μL of the GUV suspension was mixed with 1 μM of the respective peptide solution (the peptides have been labeled at the N-terminus with 5,6-carboxyfluorescein as previously described)[19] and adjusted to a final volume of 100 μL with dextran buffer in an Ibidi plate. After 30 min of incubation at room temperature, the GUVs were imaged using a BZ-X800E fluorescence microscope (Keyence, Osaka, Japan), and the images were processed with ImageJ.

RESULTS AND DISCUSSION

Design of the Peptide Library. In the first set of experiments, we examined how the antimicrobial activity of 8A is related to specific amino acid side chains in its sequence. Therefore, we generated a small library of new peptides by replacing each amino acid residue with alanine in the hydrophilic part of RL-8 and aside to the residues selected to insert the triazolyl-bridge within peptide 8A (Table S1). Peptides were synthesized using an automated SPPS approach, and peptide 8A was generated as previously described by introducing a triazolyl-bridge between L-propargylglycine and L-ε-azido-norleucine using the Cu(I)-catalyzed azide−alkyne cycloaddition click reaction (Scheme S1).[19] Particularly, we systematically replaced residues having a basic, polar, or hydrophilic nature by alanine. This resulted in peptides AA-1 (substitution of lysine 4 and 8), AA-2 (substitution of arginine 3 and 7), AA-3 (substitution of lysine 8 and 12), AA-4 (N-terminal addition of acetylated-alanine and substitution of lysine 4), and AA-5 (N-terminal acetylation of glycine 1, and substitution of arginine 7 and asparagine 11). In all the peptides, we maintained the net charge as +4, to avoid any type of influence of the net charge on the biological activity. Beside these peptides, we included also the parent peptides RL-8 and 8A as controls and for comparison in our study. All peptides presented here feature distinct distribution of hydrophobic and hydrophilic amino acids, as highlighted by their helical wheel projections (Figure 1). As mentioned above, retro-inverted peptides can have enhanced proteolytic stability. We thus additionally designed and synthesized retro-inverso (ri) variants of RL-8 and 8A leading to the peptides ri-RL-8 and ri-8A (Table S1).

Introduction of a Triazolyl-Bridge Enhances Antimicrobial Activity, and Arg3, Arg7, and Asn11 Are Important for Efficacy. All the peptides were tested against two bacterial strains, namely, Gram-positive *B. spizizenii* and Gram-negative *S. typhimurium* (Figure 2). We selected these species since antimicrobial peptides against them were previously studied and we were thus able to directly compare the observed efficacy of our peptides.[19] The peptides RL-8, AA-1, AA-3, and AA-4 all show comparable potency against Gram-positive *B. spizizenii*, whereas AA-2 and AA-5 have substantially lower antimicrobial activity, as measured by relative cell viability, which is most obvious at peptide concentrations of 5 μM and 10 μM (Figure 2A). The same result was obtained in the case of Gram-negative *S. typhimurium*, except for AA-4, which performs somewhat better than the parent peptide RL-8 and all other analogues at peptide concentrations of 0.5 μM and 1 μM (Figure 2B). In

https://doi.org/10.1021/acs.biochem.5c00101
Biochemistry 2025, 64, 3311−3321

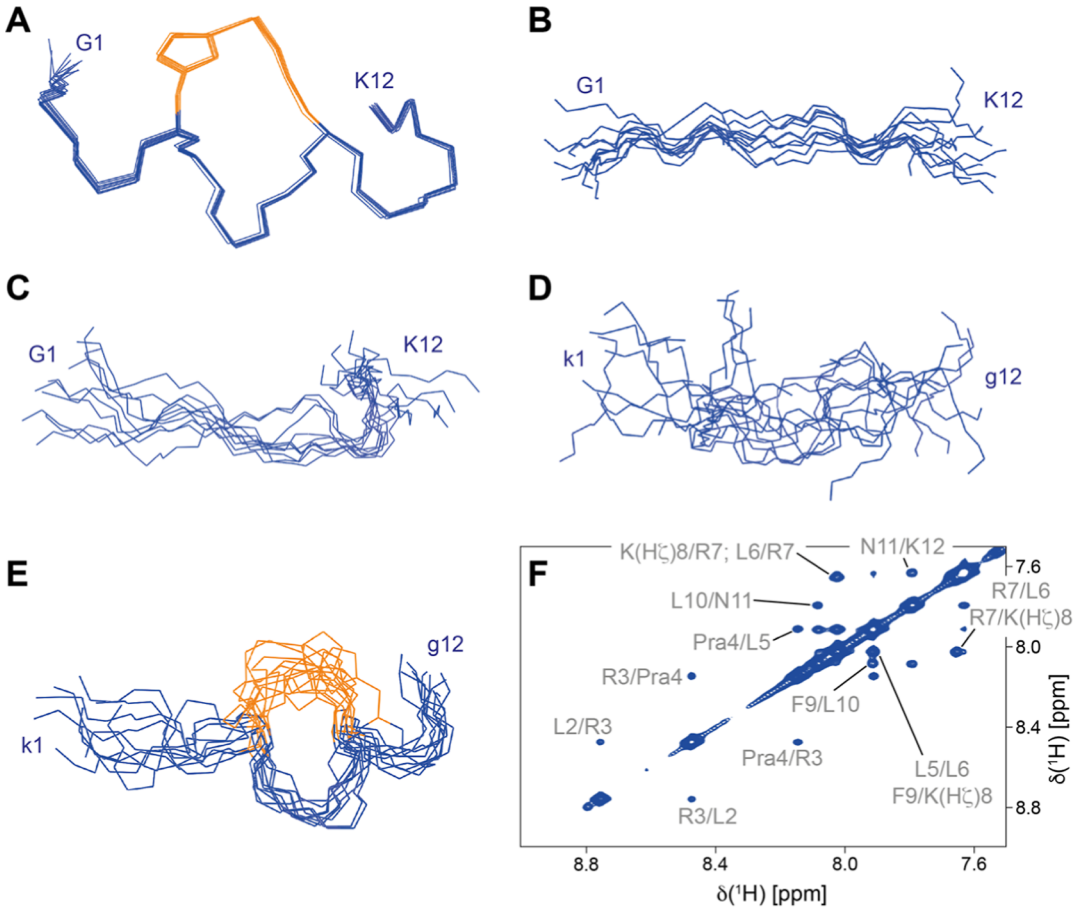

Figure 3. Conformational ensembles representing the ten lowest energy states obtained by NMR spectroscopy of the peptides (A) 8A, (B) RL-8, (C) AA-2, (D) ri-RL-8, and (E) ri-8A. Blue lines represent the peptide backbone and orange lines the side-chain triazolyl-bridge between L-propargylglycine and L-ε-azido-norleucine at amino acid positions 4 and 8, respectively. For better orientation, the N- and C-termini are indicated by one letter code and the amino acid position. (F) Amide−amide region of the 2D ^{1}H,^{1}H-NOESY spectra of 8A (measured in 90% H_2O/10% D_2O at 298 K with 500 ms NOESY mixing time at a 500 MHz NMR spectrometer). Amino acids are abbreviated based on one letter code, Pra = L-propargylglycine.

comparison to RL-8, peptide 8A performs as previously described, featuring a 2-fold and 4-fold reduction in relative cell viability against *B. spizizenii* and *S. typhimurium*, respectively, at 0.5 μM concentration (Figure 2C and 2D). We have recently compared 8A with the antimicrobial peptide LL-37, which is widely applied to address infections caused by bacteria, fungi, and viruses.[19] In these studies, 8A performed slightly less effectively than LL-37 in activity assays against methicillin-resistant *Salmonella aureus*. Also, the retro-inverso variants ri-RL-8 and ri-8A show higher efficacy than RL-8, with ri-8A having the same antimicrobial activity as 8A and ri-RL-8 being somewhat less potent than these two peptides (Figure 2C and 2D). Regarding the alanine-containing analogues in more detail, peptides AA-1, AA-3, and AA-4 show similar activities against both bacterial strains as the linear peptide RL-8, except for AA-4 being somewhat more potent against *S. typhimurium* than RL-8 as mentioned above. Consequently, substituting lysine 4, 8, or 12 by alanine or adding acetyl-alanine at the N-terminus did not substantially influence the efficacy of the peptide. We thus can conclude that these residues and extension of the peptide sequence by one more amino acid, acetyl-alanine, do not play a major role in mediating the antimicrobial activity. In contrast, peptides AA-2 and AA-5 demonstrate a significant decrease in antimicrobial activity within the range of tested concentrations (Figure 2A and 2B). Whereas this effect is not observed at lower concentrations (0.5 and 1.0 μM), it becomes obvious at 5 and 10 μM. Consequently, arginine residues 3 and 7 and asparagine 11 may be functionally relevant for the potency of the molecule. The N-terminal acetylation of glycine 1, in contrast to peptide AA-4 without extending the amino acid sequence by alanine, may play an additional role in reducing the efficacy of the peptide. This finding might suggest that the N-terminus is likely involved in the molecular mechanism of the peptide activity, however, only when the first amino acid is not alanine and/or when the sequence contains 12 and not 13 amino acids in length as AA-4 overall performs comparable to RL-8. Notably, the observed differences concerning arginine residues 3 and 7, asparagine 11, and the N-terminal acetylation of glycine 1 are more pronounced in the assay tested against *B. spizizenii* than in the one against *S. typhimurium* (Figure 2A and 2B). This might be related to the differences in cell membrane composition as well as general accessibility of the peptides to the cell membrane. At 25 μM peptide concentration, all of the peptides exhibited the same activity.

High-Resolution Peptide Structures Determined by NMR Spectroscopy. To better understand the increased antimicrobial activity achieved by introducing the triazolyl-bridge between amino acid residues at positions 4 and 8, we then determined the high-resolution structure of peptide 8A by

https://doi.org/10.1021/acs.biochem.5c00101
Biochemistry 2025, 64, 3311−3321

NMR spectroscopy (Figure 3A). The structure shows a well-defined α-helix, with three turns starting at glycine 1 and a turn-like conformation for the very C-terminal amino acids asparagine 11 and lysine 12. In the structure, we observe the expected hydrogen bonding pattern for an α-helix between the backbone amide group of residue i and the carbonyl group of i + 4. The α-helical structure is further reflected in the detected characteristic amide−amide NOE cross-peak pattern between 7.6 and 8.8 ppm ^{1}H chemical shift featuring many sequential connections along the peptide backbone (Figure 3F). To evaluate whether the structure can be correlated with antimicrobial activity, we further determined the high-resolution structure of the linear parent peptide RL-8 by NMR spectroscopy (Figure 3B). Noteworthily, the NMR structure of RL-8 is significantly different from the one of 8A; it resembles more a random-coil-like structure and does not exhibit a defined secondary structure. As expected, we also did not detect a cross-peak pattern in the amide region of the NOESY spectrum characteristic for a secondary structure such as α-helix or β-sheet (Figure S10A). Only three NOE cross-peaks between amides reflecting sequential connections were observed, namely, between those of arginine 3 and lysine 4, of leucine 10 and asparagine 11, and of asparagine 11 and lysine 12. It was then our interest to gain further insight into structural features that we could assign to the differences in activity between RL-8 and one of the peptides screened that was characterized by a minor performance. We therefore determined the high-resolution structure of peptide AA-2 as well (Figure 3C). It contains asparagine 11, which was already assumed to be important for efficacy and interaction with the target membrane;[24] therefore, we chose AA-2 and not AA-5. Peptide AA-2 contains alanine replacing arginines 3 and 7 and shows a much weaker effect on the relative cell viability, thus featuring lower antimicrobial activity (Table S1, Figures 1, 2A and 2B). Overall, the structure of AA-2 conforms to the one of RL-8, potentially with a somewhat higher tendency toward random coil formation (Figure 3C). This is not surprising as alanine at positions 3 and 7 provide a higher degree of flexibility than arginine at these positions. The observation of only one cross-peak in the amide region of the NOESY spectrum, between lysine 4 and leucine 5, is in good agreement with an even more unstructured peptide (Figure S10B). In summary, the NMR structure of 8A is considerably different from the the ones of RL-8 and AA-2. Peptide 8A adopts a well-defined α-helical structure, whereas RL-8 and AA-2 constitute random coil-like conformations. From these results, we hypothesize that preformation and rigidification of α-helicity might be one important factor to explain the high antimicrobial activity of 8A. To explain the observed comparable antimicrobial activity of retro-inverso peptides ri-RL-8 and ri-8A, we focused our attention on NMR structure determination of these peptides as well. The ten lowest energy states of ri-RL-8 as determined by NMR show highly unstructured conformations with no characteristic secondary structure element (Figure 3D). We detected five NOE cross-peaks in the amide region, all of them reflecting sequential connections, as expected for an unstructured and thus presumably highly flexible peptide (Figure S10C). Peptide ri-8A features an α-helix-like structure, however, with much higher flexibility compared to the structure of its parent peptide 8A as we observe a larger variation between the calculated low-energy states (Figure 3E). This agrees well with the observed NOE cross-peak pattern in the amide region that shows mostly sequential connections (Figure S10D).

CD Spectroscopy Confirms High-Resolution NMR Structures of All Peptides, and Chemical Modification Promotes Proteolytic Stability. To validate the secondary structures analyzed by NMR spectroscopy, we performed CD spectroscopy of all of the tested peptides. The linear peptide RL-8 as well as AA-2 and ri-RL-8 exhibit CD curves typical for random coil structures (Figure 4A). Only peptides 8A and ri-8A show CD spectra characteristic for an α-helical structure under the same conditions as the NMR experiments, i.e., in neat H_2O, with 8A displaying a substantially more distinct α-helical signature in the CD spectrum than ri-8A (Figure 4A). The retro-inverso peptides feature reversed CD spectra as they

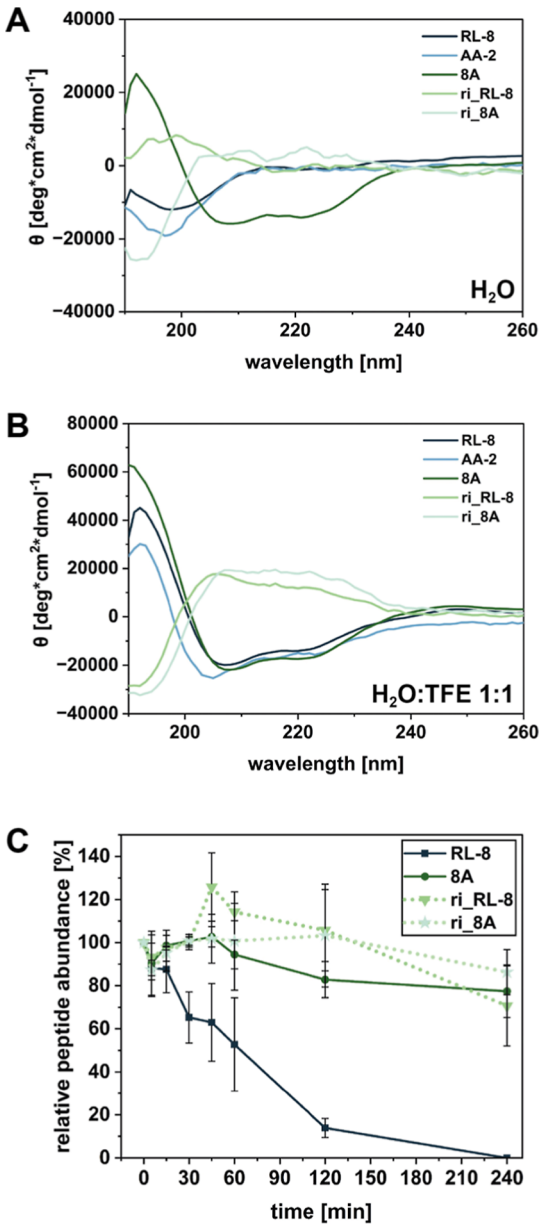

Figure 4. CD spectra of the peptides indicated by the legends recorded in (A) neat H_2O and (B) a solution of 50% TFE in H_2O. (C) Stability assay of peptides RL-8, 8A, ri-RL-8, and ri-8A in human serum. Peptide quantities were identified by acetonitrile precipitation at time points 0, 15, 30, 45, 60, 90, 120, and 240 min.

https://doi.org/10.1021/acs.biochem.5c00101
Biochemistry 2025, 64, 3311−3321

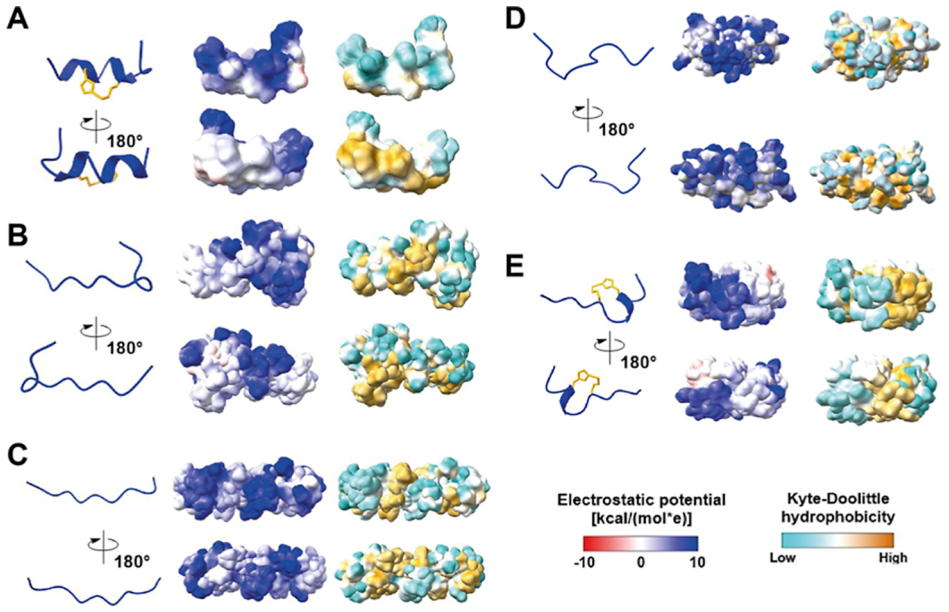

Figure 5. Structural surface characteristics of the conformational ensembles of the peptides (A) 8A, (B) AA-2, (C) RL-8, (D) ri-RL-8, and (E) ri-8A. For each peptide, the electrostatic surface potential and the surface hydrophobicity according to Kyte−Doolittle are shown, based on the scales at the bottom right. The surface orientations in each panel are related to the orientation of a representative structure from the structural ensembles shown on the left (the triazolyl-bridge in 8A and ri-8A is shown in orange).

contain D-amino acids, i.e., they are enantiomers that show properties in circular dichroism spectroscopy characteristic for optical isomers.[25] To test if these observed secondary structures can be modulated, we employed a 1:1 mixture of H_2O and trifluoroethanol (TFE), which is widely used to promote the structuring of peptides.[26,27] Under these conditions, we detected for all tested peptides CD spectra characteristic for α-helical secondary structures (Figures 4B and S11B). This result corroborates that 8A, RL-8, AA-2, ri-RL-8, and ri-8A indeed adopt the structures determined by NMR spectroscopy, and that the structures of the remaining peptides most likely resemble the ones of RL-8 and AA-2 (Figures 4A and 4B, S11A,B). α-Helix-formation of 8A in neat H_2O and of all other tested peptides in H_2O:TFE was further reflected in the expected ratio of minima in ellipticity at wavelengths of 208 and 222 nm (so-called *R*-value), which is a well-established approximation of the content of helicity (Table S7).[28] A ratio of 88.6 was calculated only for peptide 8A already in neat H_2O, supporting the idea that it forms an α-helical secondary structure in this medium. In H_2O/TFE, however, all other peptides exhibit ratios between 70 and 90, again confirming that the peptides can be forced into an α-helical structure in this medium as expected. The determined *R*-values further indicate that all peptides are in solution without aggregating, as has been shown in previous studies.[29,30] No visible signs of peptide aggregation have been observed, even at the applied concentrations for the NMR experiments. The obtained NMR spectra strongly suggest that the peptides do not aggregate, as indicated by the observed chemical shifts, line widths, and signal intensities (Figures 3F and S10, S12A,B, and Tables S2−S6, S9, and S10). To further control for potential peptide aggregation, we monitored the relative hydrophobicity based on the content of acetonitrile during HPLC-based preparation, suggesting as well that no aggregation occurs (Table S8).

As not only the secondary structure but also the incorporation of different moieties, such as the triazolyl one, can influence the stability of peptides against proteolytic degradation (thereby enhancing their antimicrobial activity through lifetime elongation), we monitored the relative peptide abundance of RL-8, 8A, ri-RL-8, and ri-8A in human serum over time (Figure 4C).[31,32] As expected, the linear, nonmodified, and unstructured RL-8 is rapidly degraded by proteases. In contrast, 8A, ri-RL-8, and ri-8A show much higher proteolytic stability, with the two retro-inverso peptides being less prone to degradation. Particularly, ri-RL-8 remains stable for up to 4 h, whereas the linear RL-8 is almost fully degraded after 120 min. These data indicate that chemical modification seems to be critical to achieving substantial proteolytic stability. The triazolyl moiety and the retro-inverso peptide sequences inhibit cleavage by proteases, as observed in earlier studies.[6,8] However, as 8A and ri-8A show the same antimicrobial activity, which is higher than the one of the unstructured ri-RL-8 that features proteolytic stability comparable to that of 8A and ri-8A, the α-helical structures of the triazolyl-bridged peptides must be fundamental for enhancing the potency against the two tested pathogens (Figures 2C,D, 3A,D,E, and 4C). To analyze this finding in more detail, we further studied the molecular surfaces of the peptides regarding their potential to interact with the cellular membrane of the target pathogen.

Molecular Surface Signatures of Peptide 8A Promote Chemical Features to Interact with Cellular Membranes. To rationalize why 8A exhibits a substantially better antimicrobial activity than RL-8, AA-2, and ri-RL-8 and performs similarly to ri-8A, we analyzed features of the molecular surface in these five peptides (Figure 5).

We first investigated the distribution of the electrostatic surface potential as the cellular membrane of the bacteria features negatively charged moieties in the head groups of phospholipids, thus providing a basis for noncovalent interaction of the peptide with the target. For peptide 8A, we observed two distinct areas of positive charge on its surface, mostly clustered on one specific side of the molecule (Figure

https://doi.org/10.1021/acs.biochem.5c00101
Biochemistry 2025, 64, 3311−3321

5A). In contrast, the positive charge on the molecular surface of peptide AA-2 is somewhat more scattered and not arranged in specific sites (Figure 5B). This is of course expected due to the substitution of arginine 3 and 7 by alanine. We therefore analyzed the positive charge distribution on the molecular surface of the parent peptide RL-8 as well (Figure 5C). Here, the positive charge is more pronounced since the overall net charge is +6 and not +4 as in 8A and AA-2. However, the positive charge is arranged in a more dispersed fashion than in 8A and AA-2. The retro-inverso linear peptide ri-RL-8 shows a similar distribution of positive charge on the molecular surface as RL-8 (Figure 5D). Interestingly, in ri-8A, the positive charge is arranged in distinct areas similar to 8A, however, at different and less well-defined locations (Figure 5E). It seems obvious that the α-helical structures of 8A and ri-8A cause clustering of positive charge on one side of the peptide, creating a positively charged area along the α-helix toward the N-terminus in case of 8A. This is not reflected by the charge distribution in ri-8A, potentially due to the higher flexibility of the structure as observed by NMR (Figure 3E). The surfaces of AA-2, RL-8, and ri-RL-8, on the contrary, exhibit positively charged spots. We thus can conclude that the α-helical structure provides a basis for establishing an extended patch of positive charge, potentially enabling the peptide to bind more efficiently to the negatively charged phosphate groups of phospholipids in the cellular target membrane. At the same time, the decreased antimicrobial activity of AA-2 compared with that of RL-8 may be predominantly due to the overall reduction in positive charge. Furthermore, these findings agree well with the high importance of arginine 3 and 7 and asparagine 11 for antimicrobial activity observed in the antimicrobial assays (Figure 2A and 2B). As already mentioned, asparagine might be important to support hydrogen-bonding within the α-helices when embedded in the membrane.[24] The higher importance of arginine for functionality compared to lysine could be related to both the higher pK_a of the guanidinium group compared to that of the amine group (pK_a of about 12.5 vs 10.5) and a higher polarity of the side chain.[33] Replacing arginine with alanine therefore decreases the polarity of the hydrophilic side chain considerably more than replacing lysine.

The effect of clustering specific molecular surface features, termed molecular surface signature, is similarly evident in the case of hydrophobicity. Peptide 8A has clearly a hydrophobic area on one side and a hydrophilic area on the opposite side of the molecule (Figure 5A). This observation is strongly in contrast to the distribution of hydrophobic and hydrophilic sites in peptides AA-2, RL-8, and ri-RL-8, where they are scattered much more randomly over the surface of the molecules (Figure 5B−D). Interestingly, the hydrophilic site on peptide 8A correlates well with the positively charged patch on the molecular surface. Thinking about an interaction with the cellular membrane of the target pathogen, this clustering of hydrophobicity in the α-helix-based peptide may promote again interaction with phosphate groups, in conjunction with the electrostatic interaction. The distinct hydrophobic site, located on the opposite side of the molecule from the hydrophilic and positively charged site, potentially plays an important role in penetrating and thereby disrupting the cellular membrane. This observation is supported by the same relative organization of positive charge, hydrophilicity, and hydrophobicity within the molecular surface of ri-8A, in which the hydrophilic site also matches the positively charged area, and the hydrophobic site is on the opposite side as in 8A (Figure 5E). In fact, our previous study revealed that installing the triazolyl-bridge in the hydrophobic part of the peptide did not lead to enhanced antibacterial potency.[19] This may be due to the somewhat hydrophilic nature of triazole, which probably disrupts hydrophobic clusters and thereby changes the hydrophobic moment of the peptide. As seen in the high-resolution NMR structure, the triazole is located opposite to the hydrophobic cluster in 8A and ri-8A (Figure 5A,E), potentially explaining the substantial increase in the antimicrobial activity of these peptides. An additional reason for this enhancement might be the larger conformational space sampled by the peptides RL-8, AA-2, and ri-RL-8. This provides a higher structural flexibility of these peptides and thus in molecular signature compared to the well-structured, α-helical peptide 8A. Even though ri-8A shows a somewhat higher flexibility than 8A, it still forms an α-helical structure (Figure 3A and 3E). The interaction of 8A and ri-8A with the target cell membrane may be therefore entropically more favored than in the case of RL-8, AA-2, and ri-RL-8, leading to the observed increase in antimicrobial activity. This effect might be particularly relevant in the case of AA-2, which has lower potency against *B. spizizenii* and *S. typhimurium* than RL-8 and ri-RL-8 (Figure 2A−D). All three linear peptides show a high degree of structural flexibility, with ri-RL-8 being the most unstructured and RL-8 being the most structured one (Figure 3B−D). In terms of entropy and comparing RL-8, AA-2, and ri-RL-8, an interaction with the target cell membrane would thus be most preferential in the case of RL-8, which is well reflected by the observed highest antimicrobial activity among these three peptides. However, ri-RL-8 shows lower tendency toward a well-ordered structure but higher efficacy than RL-8. Based on this observation, we can conclude that the higher proteolytic stability of ri-RL-8 compared to that of RL-8 is the main reason for the higher antimicrobial activity of ri-RL-8 compared to that of RL-8, compensating the effects caused by high structural flexibility.

The determined structures provide a basis for more detailed analyses on interactions of the peptides with lipids, which may be instrumental in further optimizing the peptides in future studies. We therefore tested the binding of the most effective peptide from our library, 8A, to giant unilamellar vesicles (GUVs) composed of lipids and to dodecylphosphocholine (DPC) micelles and compared our observations to the linear analogue, RL-8 (Figure S12). To analyze if RL-8 and 8A bind lipids, we performed fluorescence microscopy imaging on GUVs composed of a DOPG:DOPE lipid mixture (Figures S12A). These data show that both peptides interact with lipids and, thus, potentially with cellular target membranes. In fact, this is in good agreement with our previous studies on membrane disruption of 8A and RL-8 by transmission electron microscopy upon treatment of *B. spizizenii* and *S. typhimurium* and monitored by lactate dehydrogenase release assays.[19] To identify residues as candidates involved in membrane binding, we performed NMR experiments on 8A and RL-8 in the presence of DPC micelles, which is a well-established model system for structural studies of membranes with proteins and peptides (Figure S12B,C).[34,35] 8A clearly interacts with DPC micelles, as monitored by substantial chemical shift changes in ^{1}H,^{15}N-HSQC spectra (Figure S12B and Tables S2 and S9). We further determined the high-resolution structure of 8A in the micelle-bound state, highlighting that the α-helical structure is retained upon interaction (Figures 3A and S12B). RL-8 binds to DPC micelles as well, again evidenced

https://doi.org/10.1021/acs.biochem.5c00101
Biochemistry 2025, 64, 3311−3321

by strong chemical shift changes in the ^{1}H,^{15}N-HSQC spectra (Figure S12C and Supporting Information Tables S3 and S10). Interestingly, RL-8 adopts an α-helical structure in the micelle-bound state, whereas it is disordered when in solution without DPC (Figures 3B and S12C). This is also reflected by the change of the ^{1}H chemical shifts of RL-8 from the disordered range (between 8.0 and 8.5 ppm) without DPC to higher signal dispersion and α-helical ^{1}H chemical shifts in the presence of DPC. The observed change of disorder to α-helix upon micelle interaction supports the above-discussed idea that membrane binding of RL-8 may be entropically less favored than in the case of 8A, contributing to the lower antimicrobial activity of RL-8 (Figure 2). The chemical shifts of leucine 2, arginine 3, and asparagine 11 are very similar in the micelle-bound states of RL-8 and 8A, indicating that these residues are involved in the interaction, which agrees with our alanine scan (Figures 1, 2, and S12B,C). Based on the NMR interaction studies on DPC micelles, we cannot conclude that arginine 7 potentially interacts with membranes, and further analyzing the role of this residue may thus be useful. In both micelle-bound peptides, leucine 2 might be structurally positioned in the same chemical environment by the interaction of arginine 3 with the micelle, thus affecting its chemical shifts without directly contributing to binding. In future studies, it would be worth studying the interaction of arginine 3 and asparagine 11 with liposomes or bacterial membranes instead of micelles, and examining the relevance of arginine 7, by solid-state magic-angle-spinning NMR spectroscopy, which is a well-established approach to study peptide–membrane interactions at atomic resolution.[35,36]

CONCLUSION

In this work, we present peptides with antimicrobial activity against two bacterial species, *B. spizizenii* and *S. typhimurium*. We show that specifically, residues arginine 3 and 7 and asparagine 11 are key for the efficacy of our designed peptides. As shown in a previous study, we confirm that the potency can be further substantially enhanced by installing a triazolyl-bridge between L-propargylglycine and L-ε-azido-norleucine replacing lysine 4 and 8.[19] We further show that modification of peptides RL-8 and 8A through retro-inverse synthesis successfully addresses the problem of proteolytic degradation and maintains antimicrobial efficacy. In this context, CD spectroscopy confirms the incorporation of D-amino acids, while antimicrobial testing against *B. spizizenii* and *S. typhimurium* shows that the retro-inverso peptides exhibit similar or enhanced activity compared to their regular counterparts. Proteolytic stability tests reveal that ri-RL-8 remains intact in human serum for up to 4 h, significantly surpassing the degradation time of the linear RL-8 peptide. High-resolution structures determined by NMR spectroscopy further provide evidence that the introduced triazolyl-bridge between L-propargylglycine and L-ε-azido-norleucine replacing lysine residues 4 and 8 leads to a well-defined α-helical secondary structure of the peptide with substantially enhanced potency, whereas all tested linear peptides constitute random coils. We confirm by fluorescence microscopy imaging on GUVs that peptides RL-8 and 8A bind lipid membranes, and we identify arginine 3 and asparagine 11 by NMR analysis on DPC micelles as residues potentially involved in membrane interaction. NMR-derived structures of RL-8 and 8A in the micelle-bound state further suggest that the preformation of an α-helix enhances the antimicrobial activity. This α-helical conformation creates specific molecular signatures, in particular, an extended cluster of positive charge and hydrophilic nature opposite to a hydrophobic patch on the molecular surface, which may establish a basis for efficient interaction of the antimicrobial peptide with the cellular membrane of the target pathogen. As previously shown, 8A also shows membrane-lytic activity and thus cytotoxicity in mammalian systems, such as human red blood cells and HeLa cells.[19] In future attempts to develop antimicrobial peptides based on 8A, considering selectivity as a key aspect is therefore crucial toward potential application as AMP in the context of translational medicine.

ASSOCIATED CONTENT

Supporting Information

The Supporting Information is available free of charge at https://pubs.acs.org/doi/10.1021/acs.biochem.5c00101.

Library of designed peptides; scheme of automated SPPS; HPLC chromatograms and mass spectra of all peptides; 2D ^{1}H,^{1}H-NOESY spectra of peptides RL-8, AA-2, ri-RL-8, and ri-8A; CD spectra of peptides AA-1, AA-3, AA-4, and AA-5; NMR-based analysis of peptides 8A and RL-8 bound to DPC micelles; fluorescence microscopy of peptides 8A and RL-8 bound to GUVs; observed ^{1}H chemical shifts of peptides 8A, RL-8, AA-2, ri-RL-8, and ri-8A in H_2O and of peptides 8A and RL-8 in the presence of DPC micelles; relative hydrophobicity of peptides; and R-values from CD spectra (PDF)

AUTHOR INFORMATION

Corresponding Author

Daniel Friedrich − *Department of Chemistry and Biochemistry, University of Cologne, 50939 Cologne, Germany*; orcid.org/0009-0006-4393-5692; Email: daniel.friedrich@uni-koeln.de

Authors

Michael Quagliata − *Interdepartmental Research Unit of Peptide and Protein Chemistry and Biology, Department of Chemistry "Ugo Schiff", University of Florence, I-50019 Sesto Fiorentino, Italy*; orcid.org/0000-0003-0891-3405

Joshua Grabeck − *Institute of Biochemistry, University of Cologne, 50674 Cologne, Germany*

Kathrin König − *Department of Chemistry and Biochemistry, University of Cologne, 50939 Cologne, Germany*

Anna Maria Papini − *Interdepartmental Research Unit of Peptide and Protein Chemistry and Biology, Department of Chemistry "Ugo Schiff", University of Florence, I-50019 Sesto Fiorentino, Italy*; orcid.org/0000-0002-2947-7107

Paolo Rovero − *Interdepartmental Research Unit of Peptide and Protein Chemistry and Biology, Department of NeuroFarBa, University of Florence, I-50019 Sesto Fiorentino, Italy*; orcid.org/0000-0001-9577-5228

Ines Neundorf − *Institute of Biochemistry, University of Cologne, 50674 Cologne, Germany*; orcid.org/0000-0001-6450-3991

Complete contact information is available at: https://pubs.acs.org/10.1021/acs.biochem.5c00101

Notes

The authors declare no competing financial interest.

https://doi.org/10.1021/acs.biochem.5c00101
Biochemistry 2025, 64, 3311−3321

■ ACKNOWLEDGMENTS

We thank Daniela Naumann and Dr. Philipp Hegemann for excellent maintenance of the NMR Facility at the Department of Chemistry and Biochemistry at the University of Cologne. J.G. sincerely acknowledges financial support of the German Academic Exchange Service (DAAD). The PhD scholarship of M.Q. is funded by the "Progetto Ministeriale Dipartimenti di Eccellenza 2018−2022" (58503_DIPECC-C.U.P. B96C17000200008).

■ REFERENCES

(1) Aslam, B.; Wang, W.; Arshad, M. I.; Khurshid, M.; Muzammil, S.; Rasool, M. H.; Nisar, M. A.; Alvi, R. F.; Aslam, M. A.; Qamar, M. U.; Salamat, M. K. F.; Baloch, Z. Antibiotic Resistance: A Rundown of a Global Crisis. *Infect. Drug Resist.* **2018**, *11*, 1645−1658.

(2) Zaman, S. B.; Hussain, M. A.; Nye, R.; Mehta, V.; Mamun, K. T.; Hossain, N. A Review on Antibiotic Resistance: Alarm Bells Are Ringing. *Cureus* **2017**, *9*, No. e1403.

(3) Jackson, N.; Czaplewski, L.; Piddock, L. J. V. Discovery and Development of New Antibacterial Drugs: Learning from Experience? *J. Antimicrob. Chemother.* **2018**, *73* (6), 1452−1459.

(4) Wang, G. The Antimicrobial Peptide Database Is 20 Years Old: Recent Developments and Future Directions. *Protein Sci.* **2023**, *32* (10), No. e4778.

(5) Chen, C. H.; Lu, T. K. Development and Challenges of Antimicrobial Peptides for Therapeutic Applications. *Antibiotics* **2020**, *9* (1), 24.

(6) Doti, N.; Mardirossian, M.; Sandomenico, A.; Ruvo, M.; Caporale, A. Recent Applications of Retro-Inverso Peptides. *Int. J. Mol. Sci.* **2021**, *22* (16), 8677.

(7) Al Musaimi, O.; Lombardi, L.; Williams, D. R.; Albericio, F. Strategies for Improving Peptide Stability and Delivery. *Pharmaceuticals* **2022**, *15* (10), 1283.

(8) Gentilucci, L.; De Marco, R.; Cerisoli, L. Chemical Modifications Designed to Improve Peptide Stability: Incorporation of Non-Natural Amino Acids, Pseudo-Peptide Bonds, and Cyclization. *Curr. Pharm. Des.* **2010**, *16* (28), 3185−3203.

(9) Errante, F.; Pallecchi, M.; Bartolucci, G.; Frediani, E.; Margheri, F.; Giovannelli, L.; Papini, A. M.; Rovero, P. Retro-Inverso Collagen Modulator Peptide Derived from Serpin A1 with Enhanced Stability and Activity In Vitro. *J. Med. Chem.* **2024**, *67* (6), 5053−5063.

(10) Xuan, J.; Feng, W.; Wang, J.; Wang, R.; Zhang, B.; Bo, L.; Chen, Z.-S.; Yang, H.; Sun, L. Antimicrobial Peptides for Combating Drug-Resistant Bacterial Infections. *Drug Resistance Updates* **2023**, *68*, 100954.

(11) Kalafatovic, D.; Giralt, E. Cell-Penetrating Peptides: Design Strategies beyond Primary Structure and Amphipathicity. *Molecules* **2017**, *22* (11), 1929.

(12) Kardani, K.; Milani, A.; H Shabani, S.; Bolhassani, A. Cell Penetrating Peptides: The Potent Multi-Cargo Intracellular Carriers. *Expert Opin. Drug Delivery* **2019**, *16* (11), 1227−1258.

(13) Powers, J.-P. S.; Hancock, R. E. W. The Relationship between Peptide Structure and Antibacterial Activity. *Peptides* **2003**, *24* (11), 1681−1691.

(14) Skotland, T.; Iversen, T. G.; Torgersen, M. L.; Sandvig, K. Cell-Penetrating Peptides: Possibilities and Challenges for Drug Delivery in Vitro and in Vivo. *Molecules* **2015**, *20* (7), 13313−13323.

(15) Bechara, C.; Sagan, S. Cell-Penetrating Peptides: 20 Years Later, Where Do We Stand? *FEBS Lett.* **2013**, *587* (12), 1693−1702.

(16) Splith, K.; Neundorf, I. Antimicrobial Peptides with Cell-Penetrating Peptide Properties and Vice Versa. *Eur. Biophys. J.* **2011**, *40* (4), 387−397.

(17) Drexelius, M.; Reinhardt, A.; Grabeck, J.; Cronenberg, T.; Nitsche, F.; Huesgen, P. F.; Maier, B.; Neundorf, I. Multistep Optimization of a Cell-Penetrating Peptide towards Its Antimicrobial Activity. *Biochem. J.* **2021**, *478* (1), 63−78.

(18) Grabeck, J.; Lützenburg, T.; Frommelt, P.; Neundorf, I. Comparing Variants of the Cell-Penetrating Peptide sC18 to Design Peptide-Drug Conjugates. *Molecules* **2022**, *27* (19), 6656.

(19) Grabeck, J.; Mayer, J.; Miltz, A.; Casoria, M.; Quagliata, M.; Meinberger, D.; Klatt, A. R.; Wielert, I.; Maier, B.; Papini, A. M.; Neundorf, I. Triazole-Bridged Peptides with Enhanced Antimicrobial Activity and Potency against Pathogenic Bacteria. *ACS Infect. Dis.* **2024**, *10*, 2717.

(20) D'Ercole, A.; Sabatino, G.; Pacini, L.; Impresari, E.; Capecchi, I.; Papini, A. M.; Rovero, P. On-resin Microwave-assisted Copper-catalyzed Azide-alkyne Cycloaddition of H1-relaxin B Single Chain 'Stapled' Analogues. *Pept. Sci.* **2020**, *112* (4), No. e24159.

(21) Quagliata, M.; Stincarelli, M. A.; Papini, A. M.; Giannecchini, S.; Rovero, P. Antiviral Activity against SARS-CoV-2 of Conformationally Constrained Helical Peptides Derived from Angiotensin-Converting Enzyme 2. *ACS Omega* **2023**, *8*, 22665−22672.

(22) Klukowski, P.; Riek, R.; Güntert, P. NMRtist: An Online Platform for Automated Biomolecular NMR Spectra Analysis. *Bioinformatics* **2023**, *39* (2), btad066.

(23) Klukowski, P.; Riek, R.; Güntert, P. Rapid Protein Assignments and Structures from Raw NMR Spectra with the Deep Learning Technique ARTINA. *Nat. Commun.* **2022**, *13* (1), 6151.

(24) Thomas, F.; Niitsu, A.; Oregioni, A.; Bartlett, G. J.; Woolfson, D. N. Conformational Dynamics of Asparagine at Coiled-Coil Interfaces. *Biochemistry* **2017**, *56* (50), 6544−6554.

(25) Petit, M.-C.; Benkirane, N.; Guichard, G.; Du, A. P. C.; Marraud, M.; Cung, M. T.; Briand, J.-P.; Muller, S. Solution Structure of a Retro-Inverso Peptide Analogue Mimicking the Foot-and-Mouth Disease Virus Major Antigenic Site. *J. Biol. Chem.* **1999**, *274* (6), 3686−3692.

(26) Buck, M. Trifluoroethanol and Colleagues: Cosolvents Come of Age. Recent Studies with Peptides and Proteins. *Q. Rev. Biophys.* **1998**, *31* (3), 297−355.

(27) Khandelwal, P.; Seth, S.; Hosur, V. CD and NMR Investigations on Trifluoroethanol-Induced Step-Wise Folding of Helical Segment from Scorpion Neurotoxin. *Eur. J. Biochem.* **1999**, *264* (2), 468−478.

(28) Wang, D.; Chen, K.; Kulp, J. L.; Arora, P. S. Evaluation of Biologically Relevant Short α-Helices Stabilized by a Main-Chain Hydrogen-Bond Surrogate. *J. Am. Chem. Soc.* **2006**, *128* (28), 9248−9256.

(29) Crooks, R. O.; Rao, T.; Mason, J. M. Truncation, Randomization, and Selection: Generation of a reduced length c-Jun antagonist that retains high interaction stability. *J. Biol. Chem.* **2011**, *286* (34), 29470−29479.

(30) Kwok, S. C.; Hodges, R. S. Stabilizing and destabilizing clusters in the hydrophobic core of long two-stranded alpha-helical coiled-coils. *J. Biol. Chem.* **2004**, *279* (20), 21576−21588.

(31) Testa, C.; Papini, A. M.; Chorev, M.; Rovero, P. Copper-Catalyzed Azide-Alkyne Cycloaddition (CuAAC)-Mediated Macrocyclization of Peptides: Impact on Conformation and Biological Activity. *Curr. Top. Med. Chem.* **2018**, *18* (7), 591−610.

(32) Lu, J.; Xu, H.; Xia, J.; Ma, J.; Xu, J.; Li, Y.; Feng, J. D- and Unnatural Amino Acid Substituted Antimicrobial Peptides with Improved Proteolytic Resistance and Their Proteolytic Degradation Characteristics. *Front. Microbiol.* **2020**, *11*, 563030.

(33) André, I.; Linse, S.; Mulder, F. A. A. Residue-Specific pKa Determination of Lysine and Arginine Side Chains by Indirect 15N and 13C NMR Spectroscopy: Application to Apo Calmodulin. *J. Am. Chem. Soc.* **2007**, *129* (51), 15805−15813.

(34) Kallick, D. A.; Tessmer, M. R.; Watts, C. R.; Li, C. Y. The use of dodecylphosphocholine micelles in solution NMR. *J. Magn. Reson., Ser. B* **1995**, *109* (1), 60−65.

(35) Sani, M.-A.; Rajput, S.; Keizer, D. W.; Separovic, F. NMR techniques for investigating antimicrobial peptides in model membranes and bacterial cells. *Methods* **2024**, *224*, 10−20.

(36) Medeiros-Silva, J.; Jekhmane, S.; Paioni, A. L.; Gawarecka, K.; Baldus, M.; Swiezewska, E.; Breukink, E.; Weingarth, M. High-

https://doi.org/10.1021/acs.biochem.5c00101
Biochemistry 2025, 64, 3311−3321

resolution NMR studies of antibiotics in cellular membranes. *Nat. Commun.* **2018**, *9*, 3963.

https://doi.org/10.1021/acs.biochem.5c00101
Biochemistry 2025, 64, 3311−3321